ACS APPLIED MATERIALS & INTERFACES

Research Article

www.acsami.org

Li_2S Nanocrystals Confined in Free-Standing Carbon Paper for High Performance Lithium–Sulfur Batteries

Min Wu,[†] Yi Cui,[†] and Yongzhu Fu*[,†,‡]

[†]Department of Mechanical Engineering, Indiana University–Purdue University Indianapolis, Indianapolis, Indiana 46202, United States

[‡]Richard G. Lugar Center for Renewable Energy, Indiana University–Purdue University Indianapolis, Indianapolis, Indiana 46202, United States

ABSTRACT: Lithium sulfide (Li_2S) with a high theoretical capacity of 1166 mAh g^{-1} is a promising cathode material for Li–S batteries as it allows for the use of lithium-free anodes. However, a large overpotential (~1 V) is usually needed to activate microsized Li_2S particles due to their low electronic and ionic conductivities. Here, nano-Li_2S/carbon paper electrodes are developed via a simple Li_2S solution filtration method. Li_2S nanocrystals with a size less than 10 nm are formed uniformly in the pores of carbon paper network. These electrodes show an unprecedented low potential difference (0.1 V) in the first and following charges, also show high discharge capacities, good rate capability, and excellent cycling performance. More specifically, the nano-Li_2S/carbon nanotube paper electrodes show a reversible capacity of 634 mAh g^{-1} with a capacity retention of 92.4% at 1C rate from the 4th to 100th cycle, corresponding to a low capacity fading rate of 0.078% per cycle. These results demonstrate a facile and scalable electrode fabrication process for making high performance nano-Li_2S/carbon paper electrodes, and the superior performance makes them promising for use with lithium metal-free anodes in rechargeable Li–S batteries for practical applications.

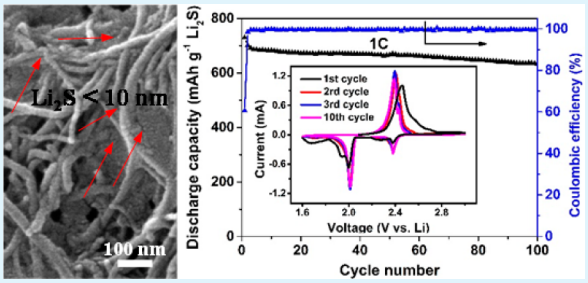

KEYWORDS: *lithium–sulfur battery, lithium sulfide, carbon paper, overpotential, electrochemical performance*

1. INTRODUCTION

High energy rechargeable batteries are in increasingly high demand owing to the increasing use of electric vehicles and portable electronics. Lithium–sulfur (Li–S) batteries, with a high theoretical specific capacity of sulfur (i.e., ~1672 mAh g^{-1}), are considered as a promising high energy density substitute of traditional lithium-ion batteries.[1−4] Sulfur as a cathode material has many benefits, such as abundance, low cost, high energy, and environmental benignity. Because of the lack of lithium in the sulfur cathode before cycling, lithium metal is usually used as the anode which has safety and cyclability issues,[5−8] impeding the commercialization of Li–S batteries. In this regard, lithium sulfide (Li_2S), the fully lithiated state of sulfur with a theoretical capacity of 1166 mAh g^{-1}, is a more desirable cathode material compared to sulfur as it could allow lithium-free anodes to be used, such as graphite, Si, Sn, and metal oxides.[9−19] Due to the low electronic conductivity, low lithium-ion diffusivity, and high charge transfer resistance of lithium sulfide, a large overpotential (~1 V) was usually observed in the initial activation of micrometer-sized Li_2S particles, which requires a high cutoff voltage of ~4.0 V in the first charge.[20,21] At this high potential, the commonly used ether-based electrolytes in Li–S batteries could be unstable and deteriorate their electrochemical performance.[22]

Recently, several Li_2S cathodes with low initial overpotential have been developed. To decrease the activation barrier of Li_2S, there are two main strategies. One is to use electrolyte additives,[20,23−26] e.g., lithium polysulfide,[20,23] redox mediators,[24] LiI,[24,26] and P_2S_5;[25] however, the effect of decreasing overpotential is not very satisfactory. The other one is to reduce Li_2S particle size to the nanoscale.[14,17,18,27−31] Unfortunately, Li_2S is highly sensitive to moisture and has a high melting point of 938 °C,[32,33] which makes it difficult to synthesize Li_2S nanoparticles. In addition, like sulfur, Li_2S also has the issue of polysulfide shuttle in Li–S cells. To fulfill the high capacity of Li_2S, a good current collector (e.g., carbon) with a favorable nanostructure which can hold polysulfides is needed in the Li_2S cathode. Currently, chemical synthesis of Li_2S–carbon nanocomposites requires multistep sophisticated processes,[14,26,28−30] including high temperature carbonization in an inert atmosphere to protect Li_2S from moisture, which are not scalable. To enable Li_2S cathodes for practical applications, a simple and scalable method is needed.

Herein, we present a facile method to uniformly distribute Li_2S nanoparticles into binder-free, free-standing multiwalled carbon nanotube (MWCNT) and carbon nanofiber (CNF) paper current collectors by a Li_2S solution filtration method. The prepared electrodes are designated as nano-Li_2S/MWCNT

Received: July 21, 2015
Accepted: September 8, 2015
Published: September 8, 2015

DOI: 10.1021/acsami.5b06615
ACS Appl. Mater. Interfaces 2015, 7, 21479−21486

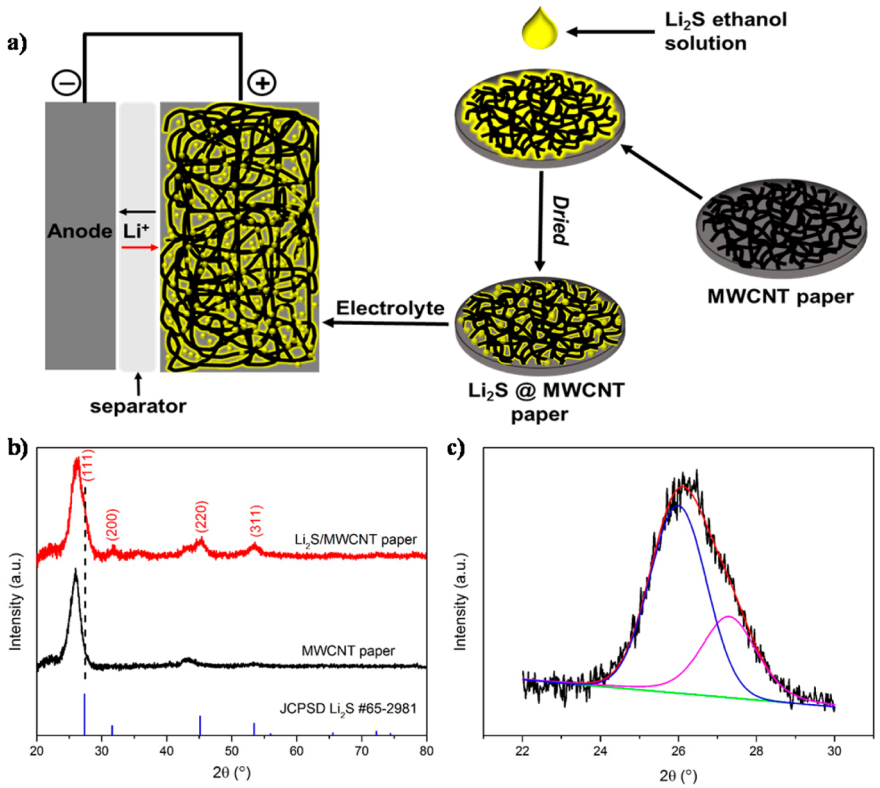

Figure 1. (a) Schematic illustration of the preparation procedure of the nano-Li_2S/MWCNT paper electrode and cell configuration; (b) XRD pattern of the blank MWCNT paper and nano-Li_2S/MWCNT electrode; (c) curve fitting of the first peak in part b.

and nano-Li_2S/CNF, respectively. This approach is inspired from our previous work on the highly reversible Li/dissolved polysulfide cell using a MWCNT paper current collector.[34] The Li_2S nanoparticles with a size of less than 10 nm are formed in the pores of carbon paper, regardless of the pore size in the carbon network. These electrodes show an unprecedented low overpotential in the first charge, high discharge capacities, good rate capability, and excellent cycling performance. This process is under low temperature, and high Li_2S loading can be achieved, making it a low cost, scalable approach.

2. EXPERIMENTAL SECTION

Materials. Lithium trifluoromethanesulfonate ($LiCF_3SO_3$, 98%, Acros Organics), lithium nitrate ($LiNO_3$, 99+%, Acros Organics), dimethoxy ethane (DME, 99+%, Acros Organics), 1,3-dioxolane (DOL, 99.5%, Acros Organics), lithium sulfide (Li_2S, 99.98%, Sigma-Aldrich), and anhydrous ethanol (99.5%, Sigma-Aldrich) were purchased and used as received.

Preparation of MWCNT and CNF Paper. An 80 mg portion of MWCNTs (Nanostructure and Amorphous Materials, Inc.) was dispersed in a miscible solution of deionized water (700 mL) and isopropyl alcohol (20 mL) by ultrasonication for 10 min, followed by vacuum filtration to render a free-standing MWCNT paper. The MWCNT paper was dried in an air-oven for 24 h at 100 °C before being peeled off and punched out into circular disks with 1.2 cm diameter (1.13 cm^2 in area, 2.2−2.4 mg in mass) for use as the current collector. The preparation of CNF (Sigma-Aldrich) paper is similar to that of the MWCNT paper.

Preparation of Nano-Li_2S/MWCNT and Nano-Li_2S/CNF Paper Electrodes and Cell Assembly. An appropriate amount of commercial lithium sulfide powder was dissolved in anhydrous ethanol in an argon-filled gloved box to form a 0.5 M Li_2S solution. The MWCNT paper was further dried at 100 °C under vacuum for 10 h to remove moisture before the preparation of nano-Li_2S/MWCNT paper electrode. First, 15 μL of Li_2S solution was added into the MWCNT paper, and then the nano-Li_2S/MWCNT electrode was dried at 40 °C inside the glovebox. The nano-Li_2S/MWCNT electrode was flipped, and additional Li_2S solution was added, and then the electrode was dried again. This procedure was repeated three times until the mass of Li_2S in the electrode was calculated to be 1 mg, corresponding to 0.9 mg cm^{-2} in the electrode. Finally, the nano-Li_2S/MWCNT electrode was dried at 100 °C in the gloved box for another 5 h to completely remove ethanol. For the cell assembly, 20 μL of electrolyte (1.0 M $LiCF_3SO_3$/0.1 M $LiNO_3$ in DME/DOL (1:1 v/v)) was added into the nano-Li_2S/MWCNT electrode, and then a Celgard 2400 separator was placed on top of the electrode, followed by additional electrolyte and lithium metal anode. Finally the cell was crimped for electrochemical evaluation on an Arbin battery cycler. For the preparation of electrodes with a Li_2S loading of 1.8 mg cm^{-2}, the Li_2S solution filtration and drying process was repeated six times, and then the Li_2S mass was accumulated to be 2 mg, corresponding to 1.8 mg cm^{-2} in the electrode. For the high Li_2S loading of 3.6 mg cm^{-2}, two layers of nano-Li_2S/MWCNT electrodes were stacked, and each has a Li_2S loading of 1.8 mg cm^{-2}. For the preparation of nano-Li_2S/CNF electrodes, a similar Li_2S solution filtration method was used, and the Li_2S loading is 0.9 mg cm^{-2}.

Characterization. The X-ray diffraction (XRD) data of the nano-Li_2S/MWCNT electrode and pristine MWCNT paper were collected on a PANalytical Empyrean X-ray diffractometer equipped with Cu Kα radiation. The samples were protected in the sample holder by Kapton tape. The scanning rate was 1° min^{-1}, and 2θ was between 20° and 80°. The XRD pattern of commercial Li_2S powder was also collected for comparison. The morphological characterizations were conducted with a JEOL JSM-7800F field emission scanning electron microscopy (SEM). The elemental mapping was performed with energy-dispersive X-ray spectroscopy (EDX) attached to the SEM.

Electrochemical Characterization. In the cycling measurements, the cells with a Li_2S loading of 0.9 mg cm^{-2} were galvanostatically charged to 2.8 V at C/20 rate in the first charge with an Arbin battery cycler, then cycled between 1.8 and 2.8 V at C/10 and C/5 rates, 1.75−2.8 V at C/2 rate, 1.65−2.8 V at 1C rate, and 1.6−2.8 V at 2C

DOI: 10.1021/acsami.5b06615
ACS Appl. Mater. Interfaces 2015, 7, 21479−21486

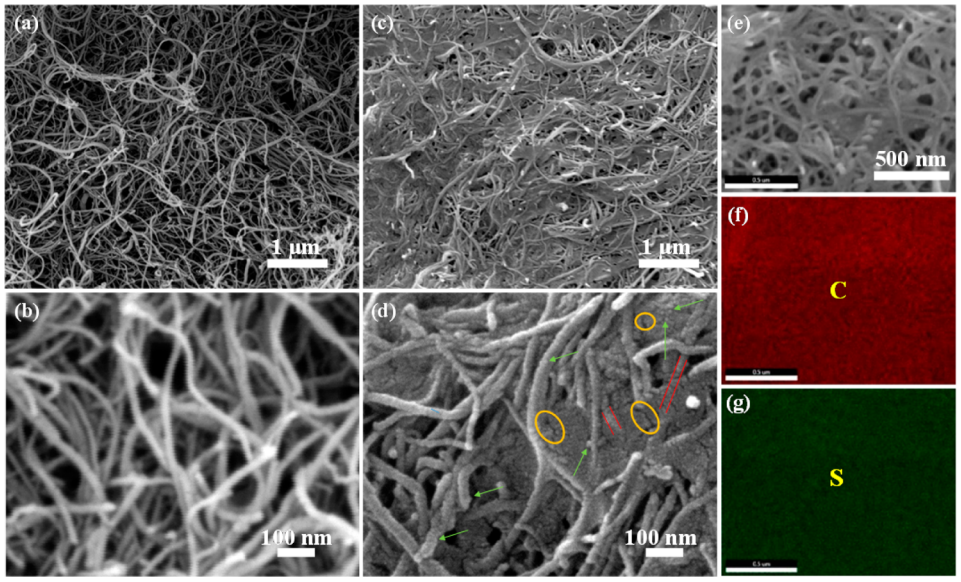

Figure 2. (a and b) SEM images of the pristine MWCNT paper, (c–e) SEM images of the freshly made nano-Li_2S/MWCNT paper electrode, and EDX mapping of carbon (f) and sulfur (g) in part e.

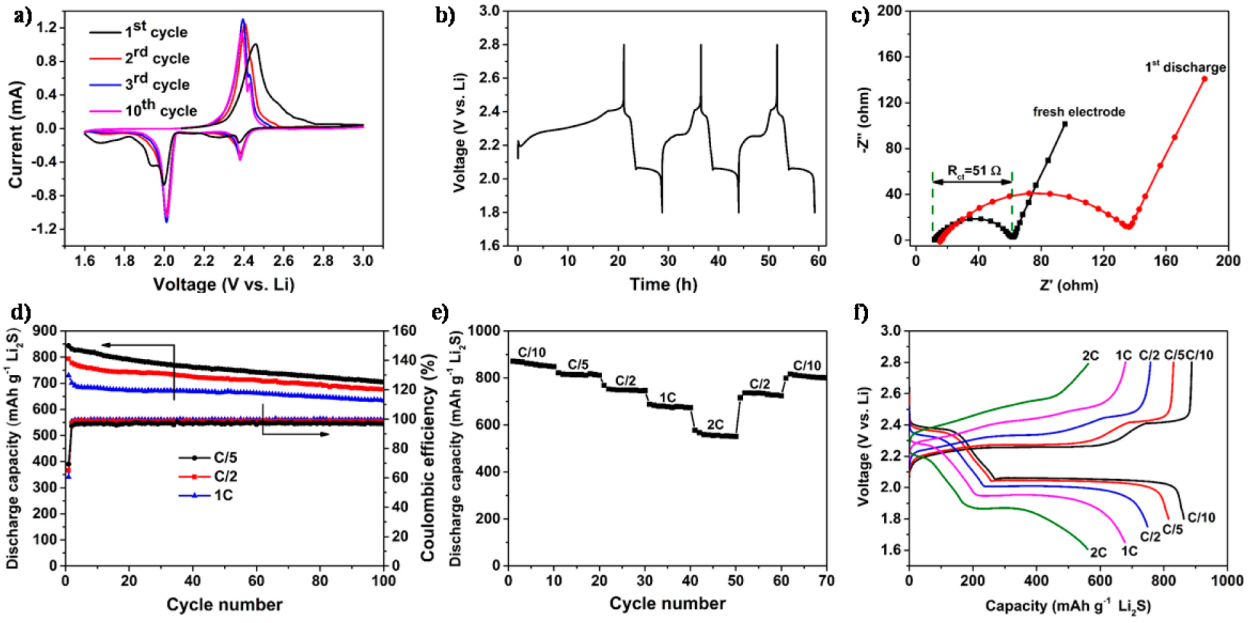

Figure 3. (a) CV of the nano-Li_2S/MWCNT electrode cycling between 1.6 and 3.0 V at a voltage scanning rate of 0.05 mV s^{-1}; (b) voltage profile, the cell was first charged at C/20 rate and then cycled at C/10 rate; (c) Nyquist plots of a cell with a nano-Li_2S/MWCNT paper electrode after freshly made (black) and after first cycle (red); (d) cyclability and Coulombic efficiency of cells at C/5, C/2, and 1C rates; (e) rate performance; (f) typical voltage versus specific capacity profiles. All the capacity are in terms of the mass of Li_2S.

rate. The dropping cutoff voltage with increasing rate is to guarantee full discharge voltage profiles due to the larger overpotential at higher rates. The cells with a Li_2S loading of 1.8 mg cm^{-2} were galvanostatically charged to 3 V at C/20 rate, and then cycled between 1.8 and 3 V at C/10. The cells with a Li_2S loading of 3.6 mg cm^{-2} were galvanostatically charged to 3 V at C/50, and then cycled between 1.65 and 3 V at C/10. The current rates and specific capacities were based on the mass of Li_2S present in the cathode (1C = 1166 mA g^{-1}). Cyclic voltammetry (CV) was performed on a Bio-Logic VSP potentiostat from open circuit voltage to 3.0 V, and then cycled between 3 and 1.6 V versus Li^+/Li at a scanning rate of 0.05 mV s^{-1}. Electrochemical impedance spectroscopy (EIS) data were collected with a Bio-Logic VSP impedance analyzer in the frequency range of 100 kHz–0.1 Hz with an applied voltage of 5 mV and Li foil as the counter and reference electrode.

3. RESULTS AND DISCUSSION

The preparation procedure of the electrode is illustrated in Figure 1a. First, commercial Li_2S powder was dissolved in anhydrous ethanol to form a homogeneous solution with a concentration of 0.5 M Li_2S, as reported by Wu et al.[35] Subsequently, a specific amount of the Li_2S solution was added into a disc of MWCNT paper, followed by drying in an argon-filled glovebox (<1 ppm of H_2O). Since the MWCNT paper has a strong absorbency to ethanol, the Li_2S solution could infiltrate throughout the MWCNT paper. Upon the evapo-

DOI: 10.1021/acsami.5b06615
ACS Appl. Mater. Interfaces 2015, 7, 21479–21486

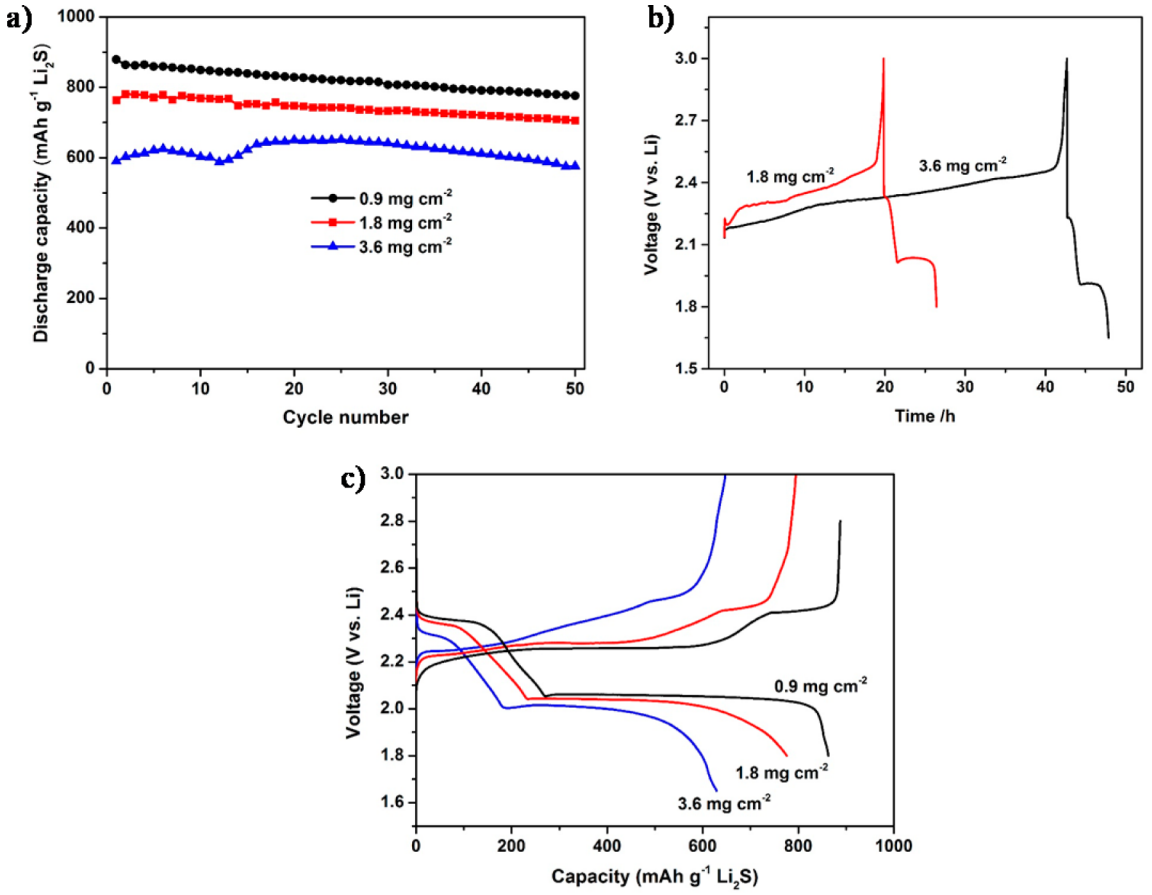

Figure 4. (a) Cyclability of the cells with different Li_2S loadings at C/10 rate. (b) Voltage versus time profile of two nano-Li_2S/MWCNT paper electrodes with different Li_2S loadings. For the Li_2S loading of 1.8 mg cm^{-2}, the cell was first charged at the C/20 rate, and then cycled between 1.8 and 3.0 V at the C/10 rate; for the Li_2S loading of 3.6 mg cm^{-2}, the cell was first charged at the C/50 rate, and then cycled between 1.65 and 3 V at the C/10 rate. (c) Voltage versus specific capacity profiles of the 5th cycles of cells with different Li_2S loadings (0.9, 1.8, and 3.6 mg cm^{-2}) at the C/10 rate.

ration of ethanol solvent, Li_2S started to nucleate. The one-dimensional (1D) structure of MWCNTs could provide nucleation sites for the formation of Li_2S particles, and the 3D porous structure of the MWCNT paper impedes Li_2S particles from agglomeration into microsized particles; therefore, the formed Li_2S particles can be in nanoscale and be uniformly dispersed in the network of the MWCNT paper.

X-ray diffraction (XRD) was performed to confirm the crystal structure of the nano-Li_2S/MWCNT electrode, and the XRD pattern is shown in Figure 1b. The XRD diffractions of Li_2S (JCPSD 65-2981) and the pristine MWCNT paper are also presented for comparison. The main peak of MWCNT is centered at around 2θ = 26.0°, which is known as the (002) crystal plane of carbon nanotubes.[36] The highest peak of Li_2S is at 2θ = 27.4°, which overlaps with the (002) plane peak of MWCNT. Figure 1c shows the curve fitting of the first peak in Figure 1b. The two deconvoluted peaks can be assigned to the (002) plane peak of MWCNT at 26.0° and the (111) plane peak of Li_2S at 27.4°, respectively. The other three major peaks of Li_2S in Figure 1b match well with the PDF data. These peaks are broad, indicating the nucleated Li_2S crystals are fairly small. According to the Scherrer equation,[37,38] the calculated size of Li_2S nanocrystals is about 7.8 nm.

Scanning electron microscopy (SEM) characterization was conducted to investigate the morphology variation between the pristine MWCNT paper and the freshly made nano-Li_2S/MWCNT electrode, as shown in Figure 2. The top view of the pristine MWCNT paper at low magnification displays the self-weaving behavior of MWCNTs and the nanoporous network of the MWCNT paper in Figure 2a. From the high magnification SEM image in Figure 2b, it can be seen that the diameter of MWCNTs is about 10−25 nm, and the size of pores is around 100−300 nm. Figure 2c−e presents the SEM images of the nano-Li_2S/MWCNT electrode; the pores of the MWCNT paper were mostly filled with Li_2S nanocrystals. The whole structure of the nano-Li_2S/MWCNT electrode is still porous, which allows efficient electrolyte penetration. The MWCNTs offer nucleation and anchoring sites for the Li_2S nanocrystals, as shown by the red parallel lines in Figure 2d. All MWCNTs are coated with Li_2S nanocrystals, forming a core−sheath structure. Obviously, the Li_2S-coated MWCNTs in Figure 2d are much thicker than the pristine MWCNTs shown in Figure 2b. To our surprise, the Li_2S particles in the pores of the MWCNT network are actually very small, most of which are less than 10 nm, as indicated by the green arrows in Figure 2d. The orange circles indicate that the nanopores still exist in the electrode, which are desirable for lithium-ion transport consequently improving the electrode kinetics. The elemental mapping of carbon (Figure 2f) and sulfur (Figure 2g) evidently validate that they are homogeneously distributed in the nano-Li_2S/MWCNT electrode. Furthermore, Figure 2g does not show

DOI: 10.1021/acsami.5b06615
ACS Appl. Mater. Interfaces 2015, 7, 21479−21486

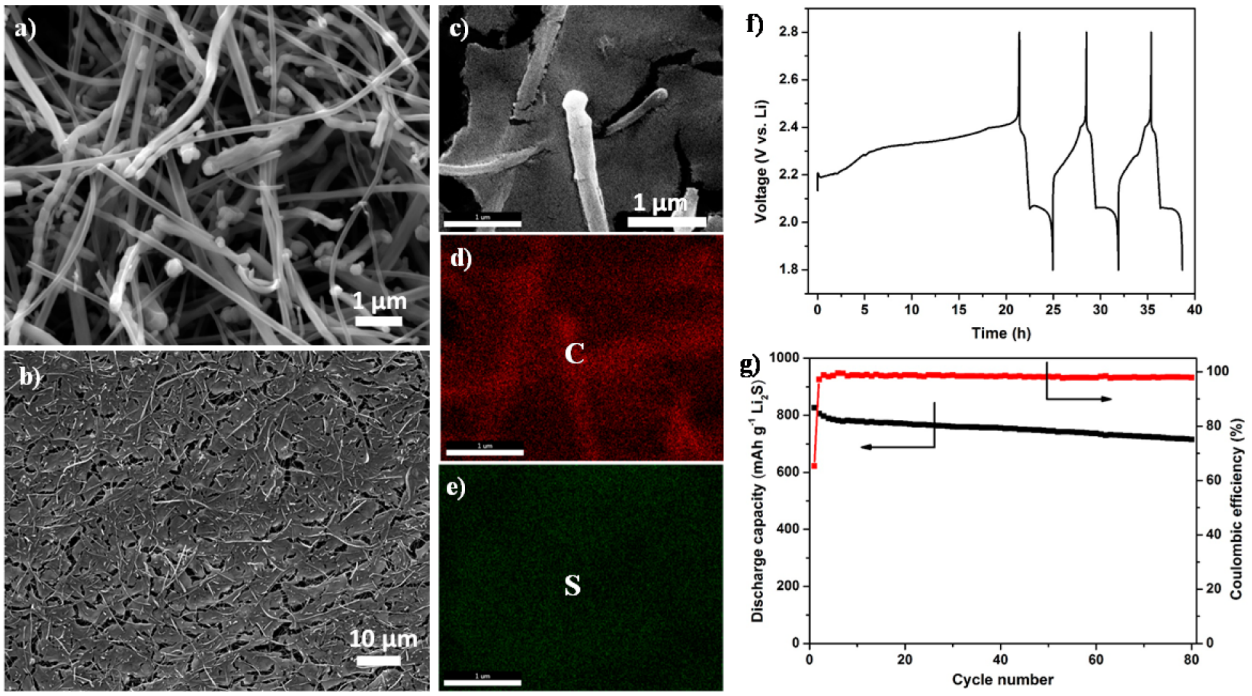

Figure 5. (a) SEM images of the pristine CNF paper; (b and c) SEM image of the freshly made nano-Li_2S/CNF electrode; EDX mapping of carbon (d) and sulfur (e) in part c; (f) voltage profile of the nano-Li_2S/CNF electrode, the cell was first charged at C/20 rate and then cycled at C/5 rate; (g) cyclability and Coulombic efficiency of the cell at C/5 rate. The capacity values are in terms of the mass of Li_2S.

agglomerated sulfur clusters, indicating that the Li_2S particles are mostly in nanoscale.

Figure 3a shows the cyclic voltammogram (CV) of a half cell with the nano-Li_2S/MWCNT electrode. The voltage was first swept from the open circuit voltage (~2.09 V) to 3 V followed by cycling between 3 and 1.6 V at a rate of 0.05 mV s^{-1}. In the first cycle, the wide anodic peak is centered at 2.48 V corresponding to the oxidation of Li_2S to polysulfides or sulfur.[33] The anodic peaks in the following cycles have shifted slightly to a lower voltage at around 2.4 V. The small potential difference (0.1 V) between the first and following cycles in CV indicates a negligible overpotential of the nano-Li_2S/MWCNT electrode, which is significantly smaller than those of microsized Li_2S crystals reported.[20,21] The anodic peak begins splitting into double peaks at ~2.38 and ~2.43 V in the third cycle, which correspond, respectively, to the transitions of Li_2S to low order polysulfides and then to high order polysulfides/sulfur.[39] In the cathodic sweep, the two peaks stay almost the same from the 2nd to the 10th cycle, revealing an excellent electrochemical stability of the nano-Li_2S/MWCNT electrode.

Figure 3b shows the voltage profile of the first three cycles of the nano-Li_2S/MWCNT electrode in a half cell. The cell was first charged to 2.8 V at C/20, and then cycled between 1.8 and 2.8 V at C/10. During the first charge, the initial charge voltage is between 2.2 and 2.45 V, which is significantly lower than those with microsized Li_2S particles under similar charge conditions,[6,7,20,21,29,40−42] indicating a negligible overpotential in the nano-Li_2S/MWCNT electrode. This result is consistent with the CV shown in Figure 3a. The following discharge exhibits two voltage plateaus which resemble the voltage profile of conventional sulfur electrodes. To understand the impedance in the nano-Li_2S/MWCNT electrode, electrochemical impedance spectroscopy (EIS) analysis was conducted on the cell. As shown in Figure 3c, the charge transfer resistance (R_{ct}) reflected by the semicircle in the high−medium frequency region in the freshly made nano-Li_2S/MWCNT electrode is only 51 Ω. In contrast, the R_{ct} significantly increases to about 121 Ω after the first cycle (discharge). The low initial R_{ct} indicates good contact between Li_2S nanocrystals and MWCNTs in the nano-Li_2S/MWCNT electrode, which consequently results in the low overpotenial in the first charge.

The cycling performance of the nano-Li_2S/MWCNT electrode with a Li_2S loading of 0.9 mg cm^{-2} at different C rates is shown in Figure 3d. The initial discharge capacities at C/5 and C/2 are 843 and 794 mAh g^{-1}, respectively. After 100 cycles, the remaining capacities are as high as 705 and 676 mAh g^{-1}, corresponding to capacity retentions of 83.6% and 85.1%, respectively. As the current density increases to 1C rate, the cycling stability improves. After the first three cycles, the discharge capacity stays as high as 92.4% from the 4th cycle to the 100th cycle, which corresponds to a low capacity fading rate of 0.078% per cycle. Moreover, starting the second cycle, the average Coulombic efficiency is around 97−99.5% over 100 cycles. The high efficiency could be ascribed to the addition of $LiNO_3$ in the electrolyte and the good reservation of polysulfides in the MWCNT paper.[34] The low efficiency in the first cycle could be due to side reactions and the formation of solid electrolyte interphase (SEI) on the surface of lithium metal anode. As the rate increases from C/5 to 1C, the efficiency slightly increases; this is because high rates weaken the shuttle effect of dissolved polysulfides by reducing the retention time of polysulfides within the electrolyte per cycle.[43]

Figure 3e presents the rate capability of the nano-Li_2S/MWCNT electrode. The cell shows high discharge capacities of 860, 814, 749, and 678 mAh g^{-1} at C/10, C/5, C/2, and 1C, respectively. Even at a high rate of 2C, the discharge capacity still can be 555 mAh g^{-1}. When the rate regained to C/10, the discharge capacity recovered to 810 mAh g^{-1} which is only marginally lower than that of the initial 10 cycles at C/10 rate, implying high reversibility of the nano-Li_2S/MWCNT elec-

DOI: 10.1021/acsami.5b06615
ACS Appl. Mater. Interfaces 2015, 7, 21479−21486

Table 1. Comparison of Electrochemical Performance of Li_2S Electrodes[a]

cathode electrode	preparation T/°C	loading (mg/cm^2)	rate	initial discharge capacity (mAh/g)	stable discharge capacity (mAh/g) and cycles	electrolyte additive	cutoff voltage (V vs Li^+/Li) of first charge	ref
				Data from This Work				
Li_2S/MWCNT paper	100	0.9	C/10	879	776 and 50 cycles	no	2.8 V at C/20	
	100	0.9	C/5	843	705 and 100 cycles	no	2.8 V at C/20	
	100	0.9	C/2	794	676 and 100 cycles	no	2.8 V at C/20	
	100	0.9	1C	729	634 and 100 cycles	no	3 V at C/20	
	100	1.8	C/10	764	705 and 50 cycles	no	3 V at C/20	
	100	3.6	C/10	590	576 and 50 cycles	no	3 V at C/40	
Li_2S/CNF paper	100	0.9	C/5	827	716 and 80 cycles	no	2.8 V at C/20	
				Data from Other Sources				
Li_2S/carbon	300	1	C/5	400	370 and 50 cycles	no	4.1 V at C/20	11
Li_2S/carbon	900	0.54	C/2	340	280 and 50 cycles	polysulfides	3 V at C/10	14
carbon coated Li_2S	550	1.7	C/50	556	270 and 50 cycles	no	3.5 V at C/50	15
Li_2S/TiS_2	400	1	C/2	666	512 and 400 cycles	no	3.8 V at C/20	17
Li_2S/carbon black	110	1	C/10	600	480 and 50 cycles	polysulfides	3.8 V at C/25	20
Li_2S/sandwich carbon	50	1	1C	620	520 and 100 cycles	no	4 V at C/20	21
Li_2S/carbon black	50	3	C/10	460	190 and 150 cycles	redox mediators	3.6 V at C/20	24
Li_2S/CNF	50	1	C/10	800	620 and 80 cycles	P_2S_5	4 V at C/20	25
Li_2S/carbon	600	0.63	C/6	410	490 and 20 cycles	no	3.5 V at C/20	27
carbon coated Li_2S	600	1.5	C/10	810	680 and 50 cycles	no	3.8 V at C/50	31
Li_2S/MWCNT	600	1	C/5	420	130 and 50 cycles	no	4 V at C/20	32
Li_2S/graphene	400	1	C/10	550	400 and 100 cycles	no	4 V at C/20	35
Li_2S/acetylene black	60	1.5	C/10	520	450 and 50 cycles	no	4.2 V at C/20	42
Li_2S/CNF	600	0.9	C/2	650	500 and 100 cycles	no	3.2 V at C/40	44
Li_2S/N-doped carbon	600	1	C/5	860	600 and 100 cycles	no	4 V at C/20	45
Li_2S/rGO	700	0.96	C/10	860	300 and 50 cycles	polysulfides	3.5 V at C/20	46

[a]The discharge capacities are based on the mass of Li_2S.

trode. Representative voltage profiles at different C-rates are shown in Figure 3f. It can be seen that the cell polarization (voltage difference between the first charge voltage plateau and the second discharge voltage plateau) slightly increases from 0.19 to 0.47 V as the rate increases from C/10 to 1C. At 2C rate, the second discharge voltage plateau is still at 1.87 V, which is higher than the values reported in the literature.[21,30] The high rate capability can be attributed to the good electrode kinetics resulting from the porous nanostructure of the Li_2S/MWCNT electrode as shown in Figure 2.

The nano-Li_2S/MWCNT electrodes with different mass loadings of Li_2S have also been evaluated. Figure 4a shows the cycle life of three cells at C/10 rate with Li_2S loadings of 0.9, 1.8, and 3.6 mg cm^{-2}, which correspond to the mass proportions of Li_2S of 30, 47, and 47 wt %, respectively, in the electrodes. For the Li_2S loading of 3.6 mg cm^{-2}, the cathode consists of two layers of nano-Li_2S/MWCNT electrodes with a Li_2S loading of 1.8 mg cm^{-2} each. Figure 4b shows the voltage versus time profile of the first cycles of the two cells with the Li_2S loadings of 1.8 and 3.6 mg cm^{-2}. Consistently, these two cells exhibit very low charge voltages (overpotential) in their first charge, which are lower than 2.4 V. As can be seen in Figure 4a, the specific capacity of Li_2S decreases as the Li_2S loading increases. For the Li_2S loading of 1.8 and 3.6 mg cm^{-2}, the initial capacities are 764 and 590 mAh g^{-1} at C/10 rate, respectively. After 50 cycles, the discharge capacities are still maintained at 705 and 576 mAh g^{-1}. A representative voltage versus capacity profile of these three cells is displayed in Figure 4c for comparison. For the high Li_2S loading of 3.6 mg cm^{-2}, the initial capacity is lower than those in the following cycles; this could be because inactive Li_2S particles within the high loading electrode could be utilized during the later cycling. High Li_2S loadings are essential for practical use, and the Li_2S loading of 3.6 mg cm^{-2} is one of the highest Li_2S loadings ever reported.

To demonstrate the versatility of this method for other self-weaving fibrous carbon current collectors, we also prepared and evaluated nano-Li_2S/CNF electrodes. CNFs are much thicker than MWCNTs, and they also form larger pores. Figure 5a shows SEM images of the pristine CNF paper. The pristine CNF paper has large pores the size of a few microns in the CNF network. After the electrode was prepared, almost all pores were filled with Li_2S crystals as shown in Figure 5b,c. Although the pores are very large, the Li_2S particles are still

DOI: 10.1021/acsami.5b06615
ACS Appl. Mater. Interfaces 2015, 7, 21479−21486

nanosized and agglomerate in the pores forming a nanoporous structure as shown in Figure 5c. The EDX spectrum in Figure 5e clearly shows that lithium sulfide is homogeneously distributed in the CNF network. This result demonstrates that only Li_2S nanoparticles instead of large Li_2S crystals can be formed by this solution filtration method, regardless of the pore size in the carbon network. The voltage profile of the nano-Li_2S/CNF electrode shown in Figure 5f is quite similar to that of the nano-Li_2S/MWCNT electrode shown in Figure 4b, presenting very low charge overpotential. The main charge voltage is below 2.4 V in the first cycle. With a Li_2S loading of 0.9 mg cm^{-2}, the nano-Li_2S/CNF paper electrode can deliver a high initial capacity of 827 mAh g^{-1} at C/5 rate and maintain a capacity retention of 86% over 80 cycles, as presented in Figure 5g. Obviously, the nano-Li_2S/CNF electrode shows comparable outstanding performance with the nano-Li_2S/MWCNT electrode. Table 1 compares the performance of nano-Li_2S/MWCNT and nano-Li_2S/CNF electrodes with other Li_2S electrodes reported in the literature. The Li_2S nanocrystals confined in carbon paper show outstanding performance in terms of initial charge voltage, specific capacity, rate capability, and cycle life.

4. CONCLUSIONS

In summary, we have successfully developed a binder-free, freestanding nano-Li_2S/carbon paper electrode via a simple Li_2S solution filtration method, of which the carbon can be MWCNT or CNF. Li_2S nanocrystals are formed as small as 10 nm and are uniformly distributed in the nanoporous carbon paper framework. The nanosized Li_2S particles together with the high conductivity of the carbon paper lead to low impedance and high performance nano-Li_2S/carbon paper electrodes with negligible overpotentials in the first charge in Li−S batteries. Both electrodes demonstrate high initial capacities and excellent cycling stability. For example, the nano-Li_2S/MWCNT electrode retained a reversible capacity of 705 mAh g^{-1} with a capacity retention of 83.6% at C/5 rate over 100 cycles. With a high Li_2S loading of 3.6 mg cm^{-2}, the electrode still exhibits a reversible capacity of 576 mAh g^{-1} at C/10 rate over 50 cycles. The nano-Li_2S/CNF electrode shows comparable performance as the nano-Li_2S/MWCNT electrode with an initial discharge capacity of 827 mAh g^{-1} at C/5 rate and a capacity retention of 86% over 80 cycles. These results demonstrate a facile and scalable electrode fabrication process for making high performance nano-Li_2S/carbon paper electrodes for high energy Li−S batteries. The superior cell performance makes them promising to be used with metal-free anodes in rechargeable Li−S batteries for practical applications.

AUTHOR INFORMATION

Corresponding Author

*Phone: +1-317-274-8983. Fax: +1-317-274-9744. E-mail: yongfu@iupui.edu.

Notes

The authors declare no competing financial interest.

ACKNOWLEDGMENTS

This work was supported by the startup grant from Purdue School of Engineering and Technology and Department of Mechanical Engineering at Indiana University−Purdue University Indianapolis (IUPUI), and summer faculty grant from Purdue Research Foundation. We would like to acknowledge the Integrated Nanosystems Development Institute (INDI) at IUPUI for use of their JEOL7800F field emission scanning electron microscope, which was awarded through NSF grant MRI-1229514. The authors also acknowledge assistance from Dr. Maren Pink and Indiana University Molecular Structure Center at Indiana University—Bloomington which is supported by the NSF Grant No. CHE-1048613 in collecting XRD data.

REFERENCES

(1) Ji, X.; Nazar, L. F. Advances in Li−S Batteries. *J. Mater. Chem.* **2010**, *20*, 9821−9826.
(2) Bruce, P. G.; Freunberger, S. A.; Hardwick, L. J.; Tarascon, J. M. Li-O_2 and Li-S Batteries with High Energy Storage. *Nat. Mater.* **2012**, *11*, 19−29.
(3) Manthiram, A.; Fu, Y.; Su, Y.-S. Challenges and Prospects of Lithium−Sulfur Batteries. *Acc. Chem. Res.* **2013**, *46*, 1125−1134.
(4) Yin, Y. X.; Xin, S.; Guo, Y. G.; Wan, L. J. Lithium−Sulfur batteries: Electrochemistry, Materials, and Prospects. *Angew. Chem., Int. Ed.* **2013**, *52*, 13186−13200.
(5) Ding, F.; Xu, W.; Graff, G. L.; Zhang, J.; Sushko, M. L.; Chen, X.; Shao, Y.; Engelhard, M. H.; Nie, Z.; Xiao, J.; Liu, X.; Sushko, P. V.; Liu, J.; Zhang, J. G. Dendrite-Free Lithium Deposition via Self-Healing Electrostatic Shield Mechanism. *J. Am. Chem. Soc.* **2013**, *135*, 4450−4456.
(6) Seh, Z. W.; Zhang, Q.; Li, W.; Zheng, G.; Yao, H.; Cui, Y. Stable Cycling of Lithium Sulfide Cathodes through Strong Affinity with a Bifunctional Binder. *Chem. Sci.* **2013**, *4*, 3673−3677.
(7) Seh, Z. W.; Wang, H.; Hsu, P.-C.; Zhang, Q.; Li, W.; Zheng, G.; Yao, H.; Cui, Y. Facile Synthesis of Li_2S−Polypyrrole Composite Structures for High-Performance Li_2S Cathodes. *Energy Environ. Sci.* **2014**, *7*, 672−676.
(8) Son, Y.; Lee, J.-S.; Son, Y.; Jang, J.-H.; Cho, J. Recent Advances in Lithium Sulfide Cathode Materials and Their Use in Lithium Sulfur Batteries. *Adv. Energy Mater.* **2015**, *5*, 201500110 DOI: 10.1002/aenm.201500110.
(9) Hassoun, J.; Scrosati, B. A High-Performance Polymer Tin Sulfur Lithium Ion Battery. *Angew. Chem., Int. Ed.* **2010**, *49*, 2371−2374.
(10) Yang, Y.; McDowell, M. T.; Jackson, A.; Cha, J. J.; Hong, S. S.; Cui, Y. New Nanostructured Li_2S/Silicon Rechargeable Battery with High Specific Energy. *Nano Lett.* **2010**, *10*, 1486−1491.
(11) Hassoun, J.; Sun, Y.-K.; Scrosati, B. Rechargeable Lithium Sulfide Electrode for a Polymer Tin/Sulfur Lithium-Ion Battery. *J. Power Sources* **2011**, *196*, 343−348.
(12) Cai, K.; Song, M. K.; Cairns, E. J.; Zhang, Y. Nanostructured Li_2S-C Composites as Cathode Material for High-Energy Lithium/Sulfur Batteries. *Nano Lett.* **2012**, *12*, 6474−6479.
(13) Fu, Y.; Zu, C.; Manthiram, A. In Situ-Formed Li_2S in Lithiated Graphite Electrodes for Lithium-Sulfur Batteries. *J. Am. Chem. Soc.* **2013**, *135*, 18044−18047.
(14) Yang, Z.; Guo, J.; Das, S. K.; Yu, Y.; Zhou, Z.; Abruña, H. D.; Archer, L. A. In Situ Synthesis of Lithium Sulfide−Carbon Composites as Cathode Materials for Rechargeable Lithium Batteries. *J. Mater. Chem. A* **2013**, *1*, 1433−1440.
(15) Jeong, S.; Bresser, D.; Buchholz, D.; Winter, M.; Passerini, S. Carbon Coated Lithium Sulfide Particles for Lithium Battery Cathodes. *J. Power Sources* **2013**, *235*, 220−225.
(16) Agostini, M.; Hassoun, J.; Liu, J.; Jeong, M.; Nara, H.; Momma, T.; Osaka, T.; Sun, Y. K.; Scrosati, B. A Lithium-Ion Sulfur Battery Based on a Carbon-Coated Lithium-Sulfide Cathode and an Electrodeposited Silicon-Based Anode. *ACS Appl. Mater. Interfaces* **2014**, *6*, 10924−10928.
(17) Seh, Z. W.; Yu, J. H.; Li, W.; Hsu, P. C.; Wang, H.; Sun, Y.; Yao, H.; Zhang, Q.; Cui, Y. Two-Dimensional Layered Transition Metal Disulphides for Effective Encapsulation of High-Capacity Lithium Sulphide Cathodes. *Nat. Commun.* **2014**, *5*, 5017−5024.

DOI: 10.1021/acsami.5b06615
ACS Appl. Mater. Interfaces 2015, 7, 21479−21486

(18) Meng, X.; Comstock, D. J.; Fister, T. T.; Elam, J. W. Vapor-Phase Atomic-Controllable Growth of Amorphous Li_2S for High-Performance Lithium Sulfur Batteries. *ACS Nano* **2014**, *8*, 10963−10972.
(19) Wang, L.; Wang, Y.; Xia, Y.-Y. Towards High Performance Lithium-Ion Sulfur Battery Based on Li_2S Cathode Using Dual-Phase Electrolyte. *Energy Environ. Sci.* **2015**, *8*, 1551−1558.
(20) Yang, Y.; Zheng, G.; Misra, S.; Nelson, J.; Toney, M. F.; Cui, Y. High-Capacity Micrometer-Sized Li_2S Particles as Cathode Materials for Advanced Rechargeable Lithium-Ion Batteries. *J. Am. Chem. Soc.* **2012**, *134*, 15387−15394.
(21) Fu, Y.; Su, Y.-S.; Manthiram, A. Li_2S-Carbon Sandwiched Electrodes with Superior Performance for Lithium-Sulfur Batteries. *Adv. Energy Mater.* **2014**, *4*, 1300655−1300659.
(22) Ryan, K. R.; Trahey, L.; Ingram, B. J.; Burrell, A. K. Limited Stability of Ether-Based Solvents in Lithium−Oxygen Batteries. *J. Phys. Chem. C* **2012**, *116*, 19724−19728.
(23) Xu, R.; Zhang, X.; Yu, C.; Ren, Y.; Li, J. C.; Belharouak, I. Paving the Way for Using Li_2S Batteries. *ChemSusChem* **2014**, *7*, 2457−2460.
(24) Meini, S.; Elazari, R.; Rosenman, A.; Garsuch, A.; Aurbach, D. The Use of Redox Mediators for Enhancing Utilization of Li_2S Cathodes for Advanced Li−S Battery Systems. *J. Phys. Chem. Lett.* **2014**, *5*, 915−918.
(25) Zu, C.; Klein, M.; Manthiram, A. Activated Li_2S as a High-Performance Cathode for Rechargeable Lithium−Sulfur Batteries. *J. Phys. Chem. Lett.* **2014**, *5*, 3986−3991.
(26) Wu, F.; Lee, J. T.; Nitta, N.; Kim, H.; Borodin, O.; Yushin, G. Lithium Iodide as a Promising Electrolyte Additive for Lithium-Sulfur Batteries: Mechanisms of Performance Enhancement. *Adv. Mater.* **2015**, *27*, 101−108.
(27) Guo, J.; Yang, Z.; Yu, Y.; Abruna, H. D.; Archer, L. A. Lithium-Sulfur Battery Cathode Enabled by Lithium-Nitrile Interaction. *J. Am. Chem. Soc.* **2013**, *135*, 763−767.
(28) Zhang, K.; Wang, L.; Hu, Z.; Cheng, F.; Chen, J. Ultrasmall Li_2S Nanoparticles Anchored in Graphene Nanosheets for High-Energy Lithium-Ion Batteries. *Sci. Rep.* **2014**, *4*, 6467−6472.
(29) Nan, C.; Lin, Z.; Liao, H.; Song, M. K.; Li, Y.; Cairns, E. J. Durable Carbon-Coated Li_2S Core-Shell Spheres for High Performance Lithium/Sulfur Cells. *J. Am. Chem. Soc.* **2014**, *136*, 4659−4663.
(30) Wu, F.; Kim, H.; Magasinski, A.; Lee, J. T.; Lin, H.-T.; Yushin, G. Harnessing Steric Separation of Freshly Nucleated Li_2S Nanoparticles for Bottom-Up Assembly of High-Performance Cathodes for Lithium-Sulfur and Lithium-Ion Batteries. *Adv. Energy Mater.* **2014**, *4*, 1400196−1400202.
(31) Suo, L.; Zhu, Y.; Han, F.; Gao, T.; Luo, C.; Fan, X.; Hu, Y.-S.; Wang, C. Carbon Cage Encapsulating Nano-Cluster Li_2S by Ionic Liquid Polymerization and Pyrolysis for High Performance Li−S Batteries. *Nano Energy* **2015**, *13*, 467−473.
(32) Wu, F.; Magasinski, A.; Yushin, G. Nanoporous Li_2S and MWCNT-linked Li_2S Powder Cathodes for Lithium-Sulfur and Lithium-Ion Battery Chemistries. *J. Mater. Chem. A* **2014**, *2*, 6064−6070.
(33) Wang, C.; Wang, X.; Yang, Y.; Kushima, A.; Chen, J.; Huang, Y.; Li, J. Slurryless Li_2S/Reduced Graphene Oxide Cathode Paper for High-Performance Lithium Sulfur Battery. *Nano Lett.* **2015**, *15*, 1796−1802.
(34) Fu, Y.; Su, Y. S.; Manthiram, A. Highly Reversible Lithium/Dissolved Polysulfide Batteries with Carbon Nanotube Electrodes. *Angew. Chem., Int. Ed.* **2013**, *52*, 6930−6935.
(35) Wu, F.; Lee, J. T.; Magasinski, A.; Kim, H.; Yushin, G. Solution-Based Processing of Graphene-Li_2S Composite Cathodes for Lithium-Ion and Lithium-Sulfur Batteries. *Part. Part. Syst. Charact.* **2014**, *31*, 639−644.
(36) Wu, M.; Wang, J.; Wu, Z.; Xin, H. L.; Wang, D. Synergistic Enhancement of Nitrogen and Sulfur Co-Doped Graphene with Carbon Nanosphere Insertion for the Electrocatalytic Oxygen Reduction Reaction. *J. Mater. Chem. A* **2015**, *3*, 7727−7731.
(37) Patterson, A. The Scherrer Formula for X-Ray Particle Size Determination. *Phys. Rev.* **1939**, *56*, 978−982.
(38) Holzwarth, U.; Gibson, N. The Scherrer Equation Versus the 'Debye-Scherrer Equation'. *Nat. Nanotechnol.* **2011**, *6*, 534−534.
(39) Barchasz, C.; Molton, F.; Duboc, C.; Lepretre, J. C.; Patoux, S.; Alloin, F. Lithium/Sulfur Cell Discharge Mechanism: an Original Approach for Intermediate Species Identification. *Anal. Chem.* **2012**, *84*, 3973−3980.
(40) Seh, Z. W.; Wang, H.; Liu, N.; Zheng, G.; Li, W.; Yao, H.; Cui, Y. High-Capacity Li_2S−Graphene Oxide Composite Cathodes with Stable Cycling Performance. *Chem. Sci.* **2014**, *5*, 1396−1400.
(41) Lin, Z.; Nan, C.; Ye, Y.; Guo, J.; Zhu, J.; Cairns, E. J. High-Performance Lithium/Sulfur Cells with a Bi-Functionally Immobilized Sulfur Cathode. *Nano Energy* **2014**, *9*, 408−416.
(42) Liu, J.; Nara, H.; Yokoshima, T.; Momma, T.; Osaka, T. Li_2S Cathode Modified with Polyvinylpyrrolidone and Mechanical Milling with Carbon. *J. Power Sources* **2015**, *273*, 1136−1141.
(43) Mikhaylik, Y. V.; Akridge, J. R. Polysulfide Shuttle Study in the Li/S Battery System. *J. Electrochem. Soc.* **2004**, *151*, A1969−A1976.
(44) Ye, F.; Hou, Y.; Liu, M.; Li, W.; Yang, X.; Qiu, Y.; zhou, l.; Li, H.; Xu, Y.; Zhang, Y. Fabrication of Mesoporous Li_2S-C Nanofibers for High Performance Li/Li_2S Cells Cathode. *Nanoscale* **2015**, *7*, 9472−9476.
(45) Chen, L.; Liu, Y.; Ashuri, M.; Liu, C.; Shaw, L. L. Li_2S Encapsulated by Nitrogen-Doped Carbon for Lithium Sulfur Batteries. *J. Mater. Chem. A* **2014**, *2*, 18026−18032.
(46) Han, K.; Shen, J.; Hayner, C. M.; Ye, H.; Kung, M. C.; Kung, H. H. Li_2S-Reduced Graphene Oxide Nanocomposites as Cathode Material for Lithium Sulfur Batteries. *J. Power Sources* **2014**, *251*, 331−337.

DOI: 10.1021/acsami.5b06615
ACS Appl. Mater. Interfaces 2015, 7, 21479−21486